Efficient Real-Time Time-Dependent Density Functional Theory Method and its Application to a Collision of an Ion with a 2D Material

Zhi Wang,[1,2] Shu-Shen Li,[1] and Lin-Wang Wang[2]
[1]State Key Laboratory for Superlattices and Microstructures, Institute of Semiconductors, Chinese Academy of Sciences, P.O. Box 912, Beijing 100083, China
[2]Materials Sciences Division, Lawrence Berkeley National Laboratory, Berkeley, California 94720, USA
(Received 24 September 2014; published 13 February 2015)

We have developed an efficient real-time time-dependent density functional theory (TDDFT) method that can increase the effective time step from <1 as in traditional methods to 0.1–0.5 fs. With this algorithm, the TDDFT simulation can have comparable speed to the Born-Oppenheimer (BO) *ab initio* molecular dynamics (MD). As an application, we simulated the process of an energetic Cl particle colliding onto a monolayer of $MoSe_2$. Our simulations show a significant energy transfer from the kinetic energy of the Cl particle to the electronic energy of $MoSe_2$, and the result of TDDFT is very different from that of BO-MD simulations.

DOI: 10.1103/PhysRevLett.114.063004 PACS numbers: 31.15.ee, 73.61.-r, 79.20.Rf

Time-dependent density functional theory (TDDFT) has been widely used from optical excitation [1–4] to ion-material collisions [5–7]. For optical excitation, the TDDFT can be solved under linear perturbation theory [8] using Casida formalism. In Ref. [9], the phonon dynamic has also been incorporated into the TDDFT in a perturbation theory. On the other hand, for many problems, direct real-time evolution of the Schrödinger's equation is necessary, e.g., to study nonlinear optical response [10], ultrafast magnetic dynamics [11], or to study an ion collision with a substrate [6,12–14]. TD-DFT can also be viewed as belonging to the general nonadiabatic molecular dynamic (NA MD) [15,16]. In the NA MD, the electron wave function follows the time-dependent Schrödinger equation, while the nuclear movement follows the classical Newton's law. The direct NA MD without introducing the energy surface hopping [17] or wave function collapsing [18] is also called Ehrenfest dynamics [19]. Compared to the adiabatic Born-Oppenheimer *ab initio* molecular dynamics (BO MD), the NA MD can be used to study problems where the electronic states are excited during the dynamics process, e.g., the carrier cooling [20], carrier transport [21,22], and charge transfer induced chemical reaction [23]. While extremely powerful, so far the real-time TDDFT suffers from its extremely high computational cost. The time step it can use is typically around 1 as, compared to 1 fs time step in BO MD. In this work, we present a new algorithm which can increase the effective time step to 0.1–0.5 fs, hence making it comparable to the BO-MD simulations.

Many algorithms have been developed in literature to evolve the wave functions directly starting from the fundamental formula $\psi_i(t+dt) = e^{-iHdt}\psi_i(t)$. Taylor expansion, split operator [24,25], and Lanczos methods [26] have been used to approximate e^{-iHdt}. But all these approximations require $|Hdt| \ll 1$ for accurate evaluation of this operator. However, since the energy spectrum width of H, especially under the flexible plane wave basis set, can be rather large (e.g., 400 eV), this results in $dt < 10^{-3}$ fs. Here, we will follow the formalism often used in quantum chemistry, expanding $\psi_i(t)$ by the adiabatic eigenstates $\varphi_l(t)$. Under the TDDFT formalism, a set of occupied single particle states $\{\psi_i(t)\}$ will be calculated following the time-dependent Schrödinger's equation:

$$i\partial\psi_i(t)/\partial t = H(t, R_j(t), \rho(t))\psi_i(t), \qquad \rho(t) = \sum_i \left|\psi_i(t)\right|^2, \tag{1}$$

where $i = 1, M$ is the index of the occupied states, and M is the number of electron. The instantaneous exchange-correlation functional approximations will be used in the $H(t, R_j(t), \rho(t))$ expression and external stimulation (e.g., external photon potential) can also be included in H. The nuclear positions $R_j(t)$ will follow:

$$M_j d^2R_j(t)/dt^2 = F_j(t), \tag{2}$$

where $F_j(t)$ is the *ab initio* force on the jth nuclear with mass M_j calculated from the DFT total energy $E(\{R_j(t)\}, \{\psi_i(t)\})$ as $F_j = -\partial E(\{R_j\}, \{\psi_i\})/\partial R_j$ (with a formula and implementation similar to that of the Hellmann-Feynman theory). Equations (1), (2) constitute an Ehrenfest dynamics [19].

To integrate Eq. (1), we will expand $\psi_i(t)$ in terms of the adiabatic eigenstates $\varphi_l(t)$:

$$\psi_i(t) = \sum_l C_{i,l}(t)\varphi_l(t) \tag{3}$$

and here $[H(t) \equiv H(t, R_j(t), \rho(t))]$

$$H(t)\varphi_l(t) = \varepsilon_l(t)\varphi_l(t). \quad (4)$$

Now, plug Eqs. (3), (4) into Eq. (1), we have

$$\dot{C}_{i,l}(t) = -i\varepsilon_l(t)C_{i,l}(t) - \sum_k C_{i,k}(t)V_{lk}(t), \quad (5)$$

where

$$V_{lk}(t) = \langle \varphi_l(t) | \partial\varphi_k(t)/\partial t \rangle. \quad (6)$$

Because of the fact that $\varepsilon_l(t)$ appears explicitly in the diagonal term in Eq. (5), the dt used to evolve Eq. (5) will no longer be limited by the energy spectrum width of H. In practice, however, the dt used to integrate Eq. (5) can still be rather small due to the off diagonal term $V_{lk}(t)$, which describes the coupling between adiabatic states l and k. The $V_{lk}(t)$ can have a very sharp peak with time, especially when couplings between l and k are weak [27]. This difficulty, however, is in a sense artificial due to the use of $\varphi_l(t)$, which can change its identity suddenly when two states anticross each other in energy [hence $\partial\varphi_k(t)/\partial t$ in Eq. (6) becomes extremely large]. In [27], we have developed an algorithm to overcome this problem. Under this algorithm, during the time interval $[t_1, t_2]$, we can use $\varphi_l(t_1)$ as the basis to represent the Hamiltonian as a matrix, then every element of this matrix within $[t_1, t_2]$ can be approximated as

$$H(t) = H(t_1) + (t - t_1)/(t_2 - t_1) \times (H(t_2) - H(t_1)) \quad (7)$$

In order to obtain the two matrices $H(t_1)$ and $H(t_2)$, all we need to have are $\{\varepsilon_l(t_1), \varphi_l(t_1)\}$ and $\{\varepsilon_l(t_2), \varphi_l(t_2)\}$. It has been shown that [27], for a typical carrier dynamics problem, Eq. (7) holds very well for $\Delta t = t_2 - t_1 \leq 0.5$ fs. Now, to integrate Eqs. (5), (6) from t_1 to t_2, a small dt ($<$ as) is used. However, within the $[t_1, t_2]$ interval, instead of solving $\{\varphi_l(t)\}$ from the original Hamiltonian [Eq. (4)] for every dt step, we solve $\{\varphi_l(t)\}$ by diagonalizing the matrix of Eq. (7), and representing $\{\varphi_l(t)\}$ with $\{\varphi_l(t_1)\}$. This requires the diagonalizing of a $N \times N$ $H_{ij}(t)$ matrix from Eq. (7) for every dt step, where N is the number of adiabatic states included in Eq. (3). A major saving comes when we truncate the number N, so it is significantly smaller than the original number of the plane wave basis function in Eq. (1) and Eq. (4) (which can be a thousand time larger than N). As a result, the computational time on the integration of Eqs. (5) and (6) is negligible compared to the time for solving Eq. (4). The actual choice of N might depend on the problems. However, for most cases, a few eV above the ground state's highest occupied adiabatic state might be good enough. For the problems to be studied later in this Letter, we have used $N = 2M$, where M is the number of occupied orbitals. More technical details can be found in Ref. [27] and in the Supplemental Material [28]. Note that, if needed, a further speed-up is possible by not diagonalizing the matrix $H_{ij}(t)$ at each dt step within $[t_1, t_2]$, but integrating $\psi_i(t)$ from Eq. (1) under the fixed basis set of $\{\varphi_l(t_1)\}$ and the $H_{ij}(t)$ of Eq. (7), and only change the basis set from $\{\varphi_l(t_1)\}$ to $\{\varphi_l(t_2)\}$ at $t = t_2$.

The above scheme has been worked out in Ref. [27]. However in Ref. [27] only one carrier wave function is integrated with time, and the nuclear force is provided by classical force fields. Here, we will consider all occupied states $\psi_i(t)$ and use the DFT atomic forces calculated from $\psi_i(t)$ for nuclei dynamics. There is however one problem that needs to be solved. When using Eq. (7), we need to know the Hamiltonian $H(t_2)$ at time t_1. This requires us to know $\rho(t_2)$ while at $t = t_1$. We have used an iterative leapfrog method to solve this problem. More specifically, at $t = t_1$, we first estimate $\rho(t_2)$ (e.g., using linear extrapolation from previous steps), then get $H(t_2)$ and $\{\varphi_i(t_2), \varepsilon_i(t_2)\}$. We will use this to carry out Eqs. (5)–(7), that will yield a new $\rho''(t_2)$. Then a mixed charge $\rho'(t_2)$ from $\rho(t_2)$ and $\rho''(t_2)$ (e.g., with the Kerker algorithm [29]) will be used as the $\rho'(t_2)$ in the next iteration. This will be repeated until $\rho''(t_2)$ and $\rho(t_2)$ are close to each other. In practice, we found that about 4 iterations are needed to get a well converged result. For the nuclear dynamics, we use the Verlet algorithm; hence, while the electronic energies and atomic forces are evaluated at t_1, t_2 points, the velocities are evaluated at the $(t_1 + t_2)/2$ point. Thus, at t_1, we know $F_j(t_1)$, hence know $V_j[(t_1 + t_2)/2]$, then $R_j(t_2)$. The total energy can be evaluated at $(t_1 + t_2)/2$, with the electronic energy at that point being the average of the values at t_1 and t_2. A good way to test the accuracy of the Ehrenfest dynamics is to check the total energy conservation during the simulation.

To test the above algorithm, we have first applied it to a few simple systems. Norm conserving pseudopotentials are used with the plane wave basis set in the original Hamiltonian. The Perdew, Burke, Ernzerhof [30] generalized gradient approximation functional is used. The ground states $\{\varphi_l(t)\}$ at each Δt step $(t_1, t_2, \ldots)$ are calculated by the conjugate gradient method as implemented in the PEtot code [31]. The evolution of Eq. (5) for different "i" in $C_{i,l}(t)$ can be carried out with different processors, resulting in high parallelization to carry out Eq. (5).

The first test system is an 8 atom cell CdSe with only the Γ point. It has 72 electrons in total, we have used 72 adiabatic states (note each state can be occupied by 2 electrons). The result of Eqs. (5)–(7) with $\Delta t = 0.2$ fs and the one integrated from a simple direct integration, $\psi_i(t + dt) = \psi_i(t) - idtH(t)\psi_i(t)$ with $dt = 10^{-5}$ fs, are shown in Fig. 1S and Fig. 2S of the Supplemental Material [28]. The difference of these two simulations is extremely small and the remaining small error comes from the nonconvergence of the direct integration method in regard to dt.

For a second test, we have calculated the light absorption spectrum of a 50 atom Au cluster using the new real time TDDFT method, and compared the result with the linear perturbation TDDFT method (using the PWscf code [32]). The excellent agreement is shown in Fig. 3S of [28]. The third test system is a $3 \times 3 \times 3$ aluminum cluster (of a 4 atom face-centered-cubic cell, hence with 108 Al atoms). An initial nuclei velocity is set according to 300 K temperature, and an initial carrier excitation from one valence state to one conduction band state is used as shown in Fig. 4S of [28]. This problem mimics a hot carrier cooling process in a metal cluster, a very important topic in plasmonic harvest of hot carriers [33,34]. The system contains 324 electrons. Here we have used 324 adiabatic states (2 electrons per state) with roughly half to be occupied. In Fig. 5S of [28], the total energy is shown together with the kinetic energy and potential energy (the DFT energy). As can be seen, the total energy is well conserved, indicating the overall high accuracy of the Ehrenfest dynamics. We do note that, to simulate a hot carrier cooling accurately, one does need to include the beyond Ehrenfest dynamics methods [17,18,27].

Finally, we have applied the TDDFT method on a chlorine atom (or ion) colliding to a monolayer of $MoSe_2$. Transition-metal dichalcogenides MeX_2, where Me stands for transition metals (Mo, W, Ti, etc.) and X for chalcogens (S, Se, Te), are important new 2D materials with potential usage in beyond CMOS electronic devices, or renewable energy applications [35–37]. One possible way to dope the system is to replace one chalcogen by one Cl or Br [38]. Such a doping process can be done in many different ways, but a standard way in the electronic industry is via ion implantation, where an ion beam directly collides with the substrate [39]. Ions and graphene collision have been simulated with TDDFT methods before [12–14].

The system studied is shown in Fig. 1. Initially, the Cl^- ion (or neutral Cl atom) is placed 5 Å away from a monolayer $MoSe_2$, but has a perpendicular 0.5 Å/fs velocity which corresponds to a kinetic energy of 460 eV. To avoid the possible small variation in the result due to random thermomovement, we have set the initial temperature to zero (although an initial room temperature would only give a negligibly small difference). A 28 atom (including Cl) 3×3 $MoSe_2$ superlattice is built with periodic boundary conditions, sampled with the Γ point only. The vertical direction dimension is 10 Å. A 30 Ry plane wave cutoff is used. 170 adiabatic states (2 electrons per state) are used, and there are 170 valence electrons for the Cl^- ion case. We have simulated 7 projectiles, all located near the center of the hexagonal ring, as indicated by the red points in Fig. 1(b). The time for the ion to travel through this system is about 26 fs; thus, we have only simulated 26 fs, although a much longer time simulation is possible. The $\Delta t\,(= t_2\text{-}t_1)$ we used is 0.1 fs. It costs about 20 h on 128 processors to simulate one 26 fs projectile. We have also considered both the Cl^- ion and neutral Cl atom collisions in order to compare with the BO-MD results, since in BO MD, there is no easy way to simulate Cl^- ion collisions (the additional electron will occupy the $MoSe_2$ conduction band state, instead of the Cl^- state).

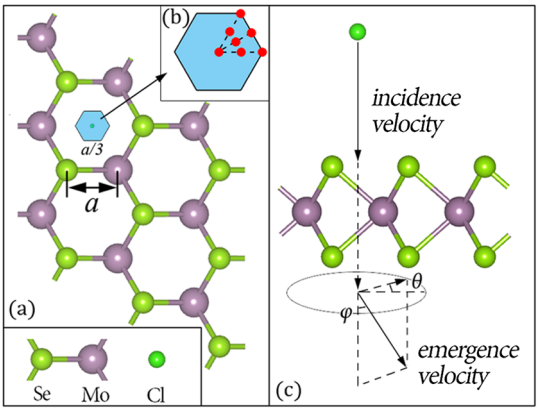

FIG. 1 (color online). Model of the Cl-$MoSe_2$ collision. a is the horizontal distance between nearest neighbors, $a = 1.890$ Å. The region of incidence has been colored blue in (a) and zoomed in (b). Red points in (b) show the initial positions of Cl. Scattering angles θ and φ are defined as shown in (c).

The projectile at the exact hexagonal central point is shown in Fig. 2. In this case, the Cl ion (or atom) passes through the $MoSe_2$ without destroying it. Three energies are shown with time: the $MoSe_2$ nuclear kinetic energy (green), the Cl nuclear kinetic energy (red), and the total electronic energy of the system (blue, this is the DFT energy at a given point). The sum of these three energies is the total energy of this system, which is a straight line (thus not shown). We first see that the Cl^- and Cl results are rather similar; thus, we will represent them with Cl in the following discussion. During the collision, the electronic

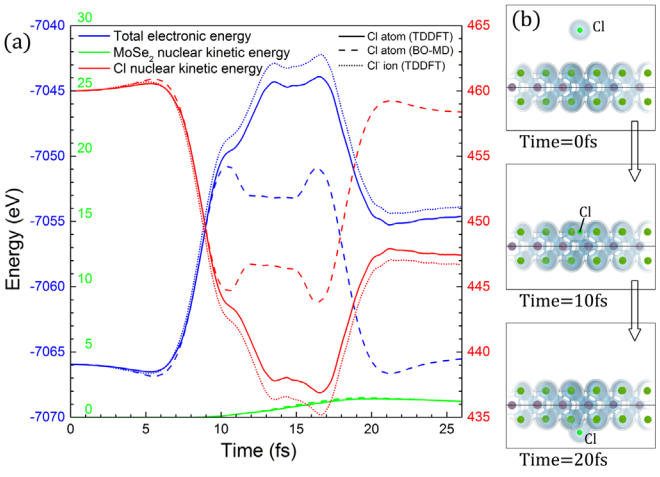

FIG. 2 (color online). (a) Electronic and nuclear kinetic energies during the central point penetration, and (b) the atom positions and charge density isosurfaces at 3 time steps.

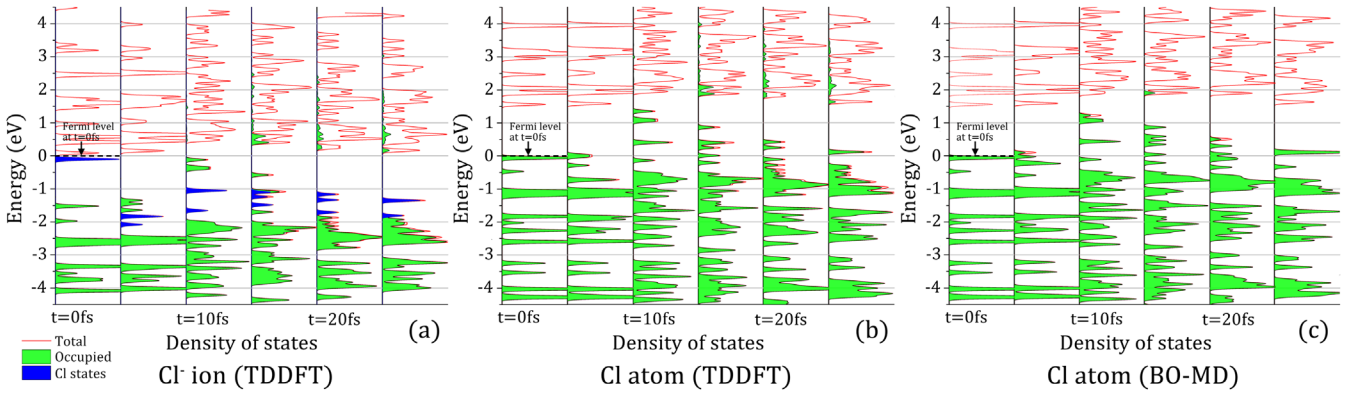

FIG. 3 (color online). Snapshots for density of states and occupations at 6 time steps, under different cases. Energy zero points are selected equal to the initial Fermi energies. Only states near Fermi energy are shown (−4.5 to 4.5 eV). Green, blue, and red states are occupied adiabatic states, Cl occupied states, and the unoccupied adiabatic state, respectively.

system of the $MoSe_2$ takes 15–24 eV from the kinetic energy of the Cl. Under BO-MD simulation, most of these electronic energies are given back to the Cl atom; thus, at the end the Cl atom only loses 1.63 eV converting to the nuclear kinetic energy of $MoSe_2$. On the other hand, for TDDFT simulation, 14 eV kinetic energy is lost for Cl, which has been converted to the electronic excitation in the $MoSe_2$ system (which cannot be described by BO MD). To better illustrate the kinetic energy loss and electron excitation in the TDDFT simulation, we have shown in Fig. 3 the electron occupation among the adiabatic density of states (DOS) [as defined by $\sum_i |C_{i,l}(t)|^2$ for each adiabatic state $\varphi_l(t)$] at 6 time steps during the collision process. We can see that, at the end of the collision, in the TDDFT simulation, there are electron occupations in the conduction band (mostly in the partial DOS of $MoSe_2$), while in BO MD, by construction, that is not allowed. These higher energy excitations account for the 14 eV kinetic energy loss. We note that in the electronic energy curve of Fig. 2, there are three sharp peaks near 10, 13, and 17 fs; they all have a width of $\tau \approx 2$ fs. These energy peaks are representations of the Hamiltonian changes, their 2 fs width corresponds to a Fourier periodicity of 4 fs, hence, an energy $E = h\omega \sim 1$ eV, which coincides with the $MoSe_2$ band gap and the excitation energy shown in Fig. 3. This means the Hamiltonian change induced by the Cl collision provides high frequency perturbation to excite the $MoSe_2$ system over its band gap. Finally, we note that there is no occupation near the upper end of the energy spectrum shown in Fig. 3, which means the $\{\varphi_l(t)\}$ truncation we have used in Eq. (3) is adequate. Meanwhile, we find a charge transfer after the collision. While the Cl^- ion loses $-0.36e$ after the collision, the neutral Cl atom only loses $-0.01e$ charge. To describe such charge transfer more rigorously, one has to go beyond the Ehrenfest dynamics, describing the charge transfer as a probabilistic event [17,18], not as a partial charge occupation in the Cl ion as in the mean field theory Ehrenfest description. Nevertheless, the charge loss does explain why the Cl^- state has lowered its energy after the collision as shown in Fig. 3(a).

For other projectiles not exactly at the center of the hexagon, their final Cl atoms will flight in slightly deflected directions and with different energy losses. This direction-energy relationship can be used experimentally to test the result of our simulation. We have fitted the simulated flight-out Cl kinetic energy as a function of the angle of emergence θ and φ [as their definitions in Fig. 1(c)] based on the 7 projectiles [Fig. 1(b)] and the symmetry considerations,

$$T_{\mathrm{Cl}}{}^{\mathrm{out}} = T_0 - \alpha(1 + \beta cos6\theta + \gamma \cos 3\theta cos6\theta)\varphi^2. \quad (8)$$

The resulting parameters of the three simulations (Cl^- with TDDFT, Cl with TDDFT, and Cl with BO MD) are shown in Table 1S of [28]. The kinetic energy loss $\Delta T_{\mathrm{Cl}} = T_{\mathrm{Cl}}{}^{\mathrm{in}}\text{-}T_{\mathrm{Cl}}{}^{\mathrm{out}}$ of the Cl^- ion with TDDFT and the Cl atom with BO MD are shown in Fig. 4. Future experiments need to be carried out to verify our results.

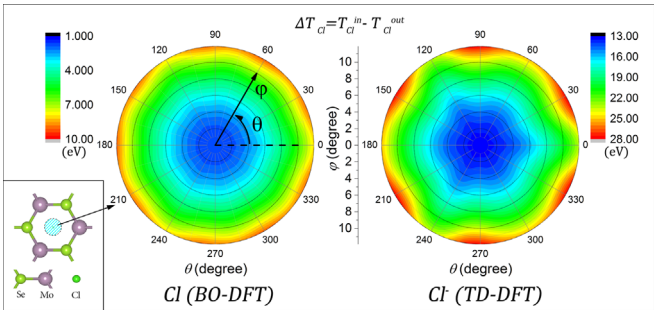

FIG. 4 (color online). Polar plots for projectile energy loss ΔT_{Cl} from Eq. (8) under different cases. From center to the peripheral, the φ changes from 0°to 12°. A diagrammatic sketch for the incidence region has been shown in the lower left corner.

This work is supported by the Director, Office of Science, Office of Basic Energy Science, Materials Science and Engineering Division, of the U.S. Department of Energy under Contract No. DE-AC02-05CH11231, through the Material Theory program in the Lawrence Berkeley National Laboratory. Z. W. is supported by the China Scholarship Council (ID:201304910244). This work uses the resource of National Energy Research Scientific Computing center (NERSC).

[1] A. Tsolakidis, D. Sánchez-Portal, and R. M. Martin, Phys. Rev. B **66**, 235416 (2002).
[2] F. De Angelis, A. Tilocca, and A. Selloni, J. Am. Chem. Soc. **126**, 15024 (2004).
[3] J. L. Bingaman, C. L. Kohnhorst, G. A. Van Meter, B. A. McElroy, E. A. Rakowski, B. W. Caplins, T. A. Gutowski, C. J. Stromberg, C. E. Webster, and E. J. Heilweil, J. Phys. Chem. A **116**, 7261 (2012).
[4] P. Cudazzo, K. O. Ruotsalainen, C. J. Sahle, A. Al-Zein, H. Berger, E. Navarro-Moratalla, S. Huotari, M. Gatti, and A. Rubio, Phys. Rev. B **90**, 125125 (2014).
[5] V. U. Nazarov, J. M. Pitarke, C. S. Kim, and Y. Takada, Phys. Rev. B **71**, 121106(R) (2005).
[6] S. Bubin, B. Wang, S. Pantelides, and K. Varga, Phys. Rev. B **85**, 235435 (2012).
[7] M. Baxter and T. Kirchner, Phys. Rev. A **87**, 062507 (2013).
[8] M. E. Casida, in *Recent Advances in Density Functional Methods, Part I*, edited by D. P. Chong (World Scientific, Singapore, 1995), p. 155.
[9] V. U. Nazarov, F. Alharbi, T. S. Fisher, and S. Kais, Phys. Rev. B **89**, 195423 (2014).
[10] Y. Takimoto, F. D. Vila, and J. J. Rehr, J. Chem. Phys. **127**, 154114 (2007).
[11] G. P. Zhang, W. Hubuer, G. Lefkidis, Y. Bai, and T. F. George, Nat. Phys. **5**, 499 (2009).
[12] Y. Miyamoto, Appl. Phys. Lett. **91**, 113120 (2007).
[13] A. V. Krasheninnikov, Y. Miyamoto, and D. Tománek, Phys. Rev. Lett. **99**, 016104 (2007).
[14] Y. Miyamoto and Hong Zhang, Phys. Rev. B **77**, 161402(R) (2008).
[15] M. Born and J. R. Oppenheimer, Ann. Phys. (Berlin) **389**, 457 (1927).
[16] R. de L. Kronig, *Band Spectra and Molecular Structure* (Cambridge University Press, New York, 1930).
[17] J. C. Tully, J. Chem. Phys. **93**, 1061 (1990).
[18] J. Bedard-Hearn, R. E. Larsen, and B. J. Schwartz, J. Chem. Phys. **123**, 234106 (2005).
[19] J. B. Delos and W. R. Thorson, Phys. Rev. A **6**, 720 (1972).
[20] S. V. Kilina, D. S. Kilin, and O. V. Prezhdo, ACS Nano **3**, 93 (2009).
[21] J. Pittner and M. J. Pederzoli, J. Phys. Chem. A **115**, 11136 (2011).
[22] I. Tavernelli, B. F. E. Curchod, and U. Roethlisberger, Chem. Phys. **391**, 101 (2011).
[23] C. F. Craig, W. R. Duncan, and O. V. Prezhdo, Phys. Rev. Lett. **95**, 163001 (2005).
[24] M. Suzuki, J. Phys. Soc. Jpn. **61**, L3015 (1992).
[25] M. Suzuki and T. Yamauchi, J. Math. Phys. (N.Y.) **34**, 4892 (1993).
[26] A. Castro, M. A. L. Marques, H. Appel, M. Oliveira, C. A. Rozzi, X. Andrade, F. Lorenzen, E. K. U Gross, and A. Rubio, Phys. Status Solidi B **243**, 2465 (2006).
[27] Junfeng Ren, N. Vukmirović, and L. W. Wang, Phys. Rev. B **87**, 205117 (2013).
[28] See Supplemental Material at http://link.aps.org/supplemental/10.1103/PhysRevLett.114.063004 for test of the new method against the conventional methods and the conservation of total energy during the dynamics.
[29] G. P. Kerker, Phys. Rev. B **23**, 3082 (1981).
[30] J. P. Perdew, K. Burke, and M. Ernzerhof, Phys. Rev. Lett. **77**, 3865 (1996).
[31] L. W. Wang, PEtot:http://cmsn.lbl.gov/html/PEtot/PEtot.html.
[32] P. Giannozzi *et al.*, J. Phys. Condens. Matter **21**, 395502 (2009).
[33] K. Zhang and H. Zhang, J. Phys. Chem. C **118**, 635 (2014).
[34] H. Xiang, X. Zhang, D. Neuhauser, and G. Lu, J. Phys. Chem. Lett. **5**, 1163 (2014).
[35] B. Radisavljevic, A. Radenovic, J. Brivio, V. Giacometti, and A. Kis, Nat. Nanotechnol. **6**, 147 (2011).
[36] I. Popov, G. Seifert, and D. Tománek, Phys. Rev. Lett. **108**, 156802 (2012).
[37] M. Chhowalla, H. S. Shin, G. Eda, L.-J. Li, K. P. Loh, and H. Zhang, Nat. Chem. **5**, 263 (2013).
[38] A. Carvalho and A. H. Castro Neto, Phys. Rev. B **89**, 081406(R) (2014).
[39] H.-P. Komsa, J. Kotakoski, S. Kurasch, O. Lehtinen, U. Kaiser, and A. V. Krasheninnikov, Phys. Rev. Lett. **109**, 035503 (2012).